Atmos. Chem. Phys. Discuss., doi:10.5194/acp-2015-911, 2016
Manuscript under review for journal Atmos. Chem. Phys.
Published: 14 March 2016

Atmospheric Chemistry and Physics Discussions

The spectral signature of cloud spatial structure in shortwave irradiance

Shi Song[1,2], K. Sebastian Schmidt[1,2], Peter Pilewskie[1,2], Michael D. King[2], Andrew K. Heidinger[3], Andi Walther[3], Hironobu Iwabuchi[4], Odele M. Coddington[2]

[1] Department of Atmospheric and Oceanic Sciences, University of Colorado, Boulder, CO, USA
[2] Laboratory for Atmospheric and Space Physics, University of Colorado, Boulder, CO, USA
[3] NOAA Center for Satellite Applications and Research, Madison, WI, USA
[4] Center for Atmospheric and Oceanic Studies, Tohoku University, Japan

Abstract

We found that cloud spatial structure manifests itself as spectral signature in shortwave irradiance fields – specifically in transmittance and net horizontal photon transport in the visible and near-ultraviolet wavelength range. In this paper, we demonstrate this through radiative transfer calculations with cloud imagery from a field experiment, and show that such three-dimensional effects may occur on scales up to 60 kilometers. Neglecting net horizontal photon transport leads to a transmittance bias on the order of ±12-19% even at the relatively coarse spatial resolution of 20 kilometers, and of more than ±50% for 1 kilometer. This poses a problem for radiative energy budget estimates from space because the bias for any pixel depends on its spatial context in a non-trivial way. The key for solving this problem may lie in the spectral dimension, since we found a robust correlation between the magnitude of net horizontal photon transport (H) and its spectral dependence (slope). It is scale-invariant and holds for the entire pixel population of a domain. This was at first surprising given the large degree of spatial inhomogeneity, but seems to be valid for any cloud field. We prove that the underlying physical mechanism for this phenomenon is molecular scattering in conjunction with cloud inhomogeneity. On this basis, we developed a simple parameterization through a single parameter ε, which quantifies the characteristic spectral signature of spatial heterogeneities. In a companion paper, we will show

Atmos. Chem. Phys. Discuss., doi:10.5194/acp-2015-911, 2016
Manuscript under review for journal Atmos. Chem. Phys.
Published: 14 March 2016

Atmospheric Chemistry and Physics Discussions

that it is accompanied by spectral radiance perturbations, which can be detected from multi-spectral imagers and may be translated into bias reductions for cloud radiative effect estimates in the future.

1. Introduction

Determining cloud radiative effects for scenes with a high degree of spatial complexity remains one of the most persistent problems in atmospheric radiation, especially at the surface where satellite observations can only be used indirectly to infer energy budget terms. In the shortwave (solar) spectral range, it is especially challenging to derive consistent albedo, absorption, and transmittance from spaceborne, aircraft, and ground-based observations for inhomogeneous cloud conditions (Kato et al., 2013; Ham et al., 2014). This problem is closely related to the long-debated discrepancy between observed and modeled cloud absorption (Stephens et al., 1990) since energy conservation for a three-dimensional (3D) atmosphere (Marshak and Davis, 2005, Eq. 12.13)

$$R + T = 1 - (A + H) \quad (1)$$

connects reflectance[1] R, transmittance T, and absorptance A of a layer. The term H accounts for lateral net radiative flux from pixel to pixel (which we will call net horizontal photon transport[2]). Out of necessity, most algorithms for deriving R, T, and A from passive imagery inherently presume isolated pixels by relying on one-dimensional (1D) radiative transfer (independent pixel approximation) which does not reproduce H. Net horizontal photon transport has therefore long been a common explanation not only for inconsistencies between measured and calculated broadband cloud absorption (Fritz and MacDonald, 1951; Ackerman and Cox, 1981) but also for remote sensing artifacts (Platnick, 2001).

Observational evidence for this explanation emerged with the availability of spectrally

[1] albedo for reflected irradiance (flux density).

[2] Our use of the term "photon" is rooted in Monte Carlo radiative transfer.

Atmos. Chem. Phys. Discuss., doi:10.5194/acp-2015-911, 2016
Manuscript under review for journal Atmos. Chem. Phys.
Published: 14 March 2016

Atmospheric Chemistry and Physics Discussions

resolved aircraft measurements of shortwave irradiance (Solar Spectral Flux Radiometer, SSFR: Pilewskie et al., 2003). Schmidt et al. (2010) derived *apparent absorption*, the sum of A and H, from irradiance measurements aboard the NASA ER-2 and DC-8 aircraft that flew along a collocated path above and below a heterogeneous anvil cloud during the Tropical Composition, Cloud and Climate Coupling Experiment (TC^4) (Toon et al., 2010). The spectral dependence of apparent absorption as well as its pixel-to-pixel variability showed that in absolute terms, H at visible wavelengths (where cloud and gas absorption are negligible) can assume similar values as the absorbed irradiance A at near-infrared wavelengths (where $|H| \ll A$). Horizontal photon transport thus has the potential to mimic substantially enhanced absorption in broadband measurements. Three-dimensional (3D) calculations confirmed the measurements, and radiative closure was achieved within measurement and model uncertainties without invoking proposed enhanced gas absorption (Arking, 1999) or big cloud droplets (Wiscombe et al., 1984). The results also suggested that the overestimation of absorption would persist even when averaging over long distances as proposed by Titov (1998). This is simply because radiation flight legs are often preferentially targeted at cloudy regions ($\langle H \rangle > 0$) and do not adequately sample clear-sky areas where photons are depleted ($\langle H \rangle < 0$), which is interpreted as *apparent emission* in measurements.

Perhaps the most significant finding by Schmidt et al. (2010) was the distinct spectral shape of H from the near-ultraviolet well into the visible wavelength range, leading to the notion of "colored" net horizontal photon transport (Schmidt et al., 2014).[3] Strategies for mitigating the overestimation of cloud absorption (Ackerman and Cox, 1981; Marshak et al., 1999) require that H be more or less constant in the visible wavelength range (Welch et al., 1980), and so the

[3] A previous study addressing horizontal photon transport from an energy budget point of view (Kassianov and Kogan, 2002) had focused on the wavelength range of 0.7-2.7 μm, specifically to avoid molecular scattering at shorter wavelengths.

Atmos. Chem. Phys. Discuss., doi:10.5194/acp-2015-911, 2016
Manuscript under review for journal Atmos. Chem. Phys.
Published: 14 March 2016

Atmospheric Chemistry and Physics Discussions

discovery of the spectral dependence of H suggested that they should be applied with caution.[4]

Further analysis of the relationship between cloud structure and its spectral signature, presented here, revealed a surprisingly robust correlation between the *magnitude* of H and its *spectral slope,* $dH/d\lambda$. In the course of this paper, we provide evidence for molecular scattering as the physical mechanism behind this correlation and develop a simple parameterization based on this knowledge. In an accompanying paper (Song et al., 2015), we will demonstrate that cloud spatial inhomogeneities also manifest themselves in spectral *radiance* perturbations via $dH/d\lambda$, which can be used for deriving H correction terms for cloud radiative effects of inhomogeneous scenes from space-borne observations.

We complete our paper by examining at which spatial aggregation H can be ignored and whether the discovered correlation between H and $dH/d\lambda$ is scale invariant. Finally, we consider the ramifications of our findings on the shortwave surface energy budget and find that while cloud transmittance biases may be significant even after spatial averaging, they are also accompanied by spectral perturbations similar to the ones we encountered for H. These biases may thus be detectable and correctable using adequate ground-based radiometers.

Following this introduction, we provide definitions of relevant terms and explain how H relates to top-of-atmosphere (TOA) and surface cloud radiative effects (CRE). We then discuss the data and model calculations that lay the basis for our study (Sections 3 and 4). In section 5, we discuss the correlations between H and $dH/d\lambda$, followed by the underlying physical mechanism and parameterization presented in Section 6. The discovered relationship is then examined as a function of spatial scale (Section 7) and interpreted in terms of the surface CRE (Section 8). In the conclusions, we discuss the significance of our findings and propose multi-spectral or spectral techniques for deriving first-order correction factors in CRE estimates from space, aircraft, and from the surface that may render 3D calculations unnecessary.

[4] For example, Marshak et al. (1999) in their conditional sampling technique require that $H = 0$ for at least two different wavelengths. Kindel et al. (2011) applied such a modified scheme for boundary layer clouds.

Atmos. Chem. Phys. Discuss., doi:10.5194/acp-2015-911, 2016
Manuscript under review for journal Atmos. Chem. Phys.
Published: 14 March 2016

Atmospheric Chemistry and Physics Discussions

2. Net horizontal photon transport and cloud radiative effect

The instantaneous radiative effect of any atmospheric constituent is the difference of net irradiance (flux density) in its presence (all-sky) and absence (clear-sky). For clouds, we define

$$CRE_\lambda = \left[\frac{\left(F_\lambda^\downarrow - F_\lambda^\uparrow\right)_{all-sky}}{F_\lambda^{\downarrow,TOA}} - \frac{\left(F_\lambda^\downarrow - F_\lambda^\uparrow\right)_{clear-sky}}{F_\lambda^{\downarrow,TOA}} \right] \times 100\%, \quad (2)$$

where $F_\lambda^\downarrow$ and $F_\lambda^\uparrow$ are downwelling and upwelling irradiance and their difference is net irradiance. For this paper, we normalize the *absolute* radiative effect by the TOA downwelling irradiance $\left(F_\lambda^{\downarrow,TOA}\right)$ and consider the *relative* radiative effect as percentage of the incident irradiance. Also, we use spectrally resolved rather than broadband quantities, indicated by subscript λ.

The TOA shortwave CRE is always negative (*cooling* effect) because the reflected irradiance $F_\lambda^{\uparrow,TOA}$ in presence of clouds is larger than for clear-sky conditions. The surface shortwave CRE is also negative because clouds decrease the transmitted irradiance $F_\lambda^{\downarrow,SUR}$, at least for homogeneous conditions; broken clouds can locally increase surface insolation. In contrast to the shortwave CRE at TOA and at the surface, homogeneous clouds have a *warming* effect on the layer in which they reside. This can be quantified in terms of the layer property absorptance

$$A_\lambda = \left[\frac{F_\lambda^{\downarrow,top} - F_\lambda^{\uparrow,top}}{F_\lambda^{\downarrow,top}} - \frac{F_\lambda^{\downarrow,base} - F_\lambda^{\uparrow,base}}{F_\lambda^{\downarrow,top}} \right] \times 100\% \quad (3)$$

for a cloud located between h_{top} and h_{base} with the same normalization as used above for the relative CRE. It can be determined from aircraft measurements by collocated legs above and below the cloud (Schmidt et al., 2010). The warming within the layer arises from absorption ($A > 0$) primarily in the near-infrared wavelength range (1 µm < λ < 4 µm). Similarly, as absorptance, layer transmittance and reflectance are defined as

$$T_\lambda = \left(\frac{F_\lambda^{\downarrow,base}}{F_\lambda^{\downarrow,top}} \right) \times 100\% \quad (4)$$

Atmos. Chem. Phys. Discuss., doi:10.5194/acp-2015-911, 2016
Manuscript under review for journal Atmos. Chem. Phys.
Published: 14 March 2016

Atmospheric Chemistry and Physics Discussions

and $R_\lambda = \left(\frac{F_\lambda^{\uparrow,top} - F_\lambda^{\uparrow,base}}{F_\lambda^{\downarrow,top}} \right) \times 100\%$. (5)

Related to layer reflectance is the albedo $\alpha_\lambda = F_\lambda^{\uparrow} / F_\lambda^{\downarrow}$ (identical to R_λ for zero surface albedo). The sum of layer absorptance, transmittance, and reflectance defined in this way is 100% and thus satisfies energy conservation for horizontally homogeneous layers. For individual pixel sub-volumes within an inhomogeneous layer (voxels), A_λ in Eq. (3) can be replaced with $A_\lambda + H_\lambda \equiv V_\lambda$ where V_λ stands for the vertical flux divergence (the net irradiance difference above and below a layer). In this way, energy conservation including horizontal transport [Eq. (1)] is retained.

The difference of the CRE at TOA and at the surface from Eq. (2) can be related to Eq. (3) as follows:

$$CRE^{TOA} - CRE^{surface} = \left[\frac{\left(F_\lambda^{net,cloud} - F_\lambda^{net,clear} \right)^{TOA}}{F_\lambda^{\downarrow,TOA}} - \frac{\left(F_\lambda^{net,cloud} - F_\lambda^{net,clear} \right)^{surface}}{F_\lambda^{\downarrow,TOA}} \right] \times 100\% \quad (6a)$$

$$= \left[\frac{\left(F_\lambda^{net,TOA} - F_\lambda^{net,surface} \right)^{cloud}}{F_\lambda^{\downarrow,TOA}} - \frac{\left(F_\lambda^{net,TOA} - F_\lambda^{net,surface} \right)^{clear}}{F_\lambda^{\downarrow,TOA}} \right] \times 100\% \quad (6b)$$

The first term inside the brackets of Eq. (6b) is identical to A_λ from Eq. (3) if the boundaries of the layer h_{top} and h_{base} are extended to the TOA and surface, respectively. We denote this by $\hat{A}_\lambda$ and distinguish full-column properties using a hat ($\hat{A}$, $\hat{H}$, $\hat{R}$, $\hat{T}$) from the layer properties that bracket only the cloud itself (A, H, R, T). The second term in Eq. (6b) stems from "clear-sky" absorption by atmospheric constituents other than clouds (gases and aerosols). Eq. (6b) can then be re-written as

$$\hat{A}_\lambda = CRE^{TOA} - CRE^{surface} + \left[\frac{\left(F_\lambda^{net,TOA} - F_\lambda^{net,surface} \right)^{clear}}{F_\lambda^{\downarrow,TOA}} \right] \times 100\% \quad (6c)$$

which simply means that the total atmospheric column absorption comprises contributions from

Atmos. Chem. Phys. Discuss., doi:10.5194/acp-2015-911, 2016
Manuscript under review for journal Atmos. Chem. Phys.
Published: 14 March 2016

the cloud itself as well as from clear-sky absorption.[5] In presence of horizontal inhomogeneities, the left and right side of Eq. (6c) may be inconsistent unless $\hat{A}_\lambda$ is replaced with $\hat{V}_\lambda = \hat{A}_\lambda + \hat{H}_\lambda$ as above.

Presented in this way, the central role of absorptance and horizontal transport in linking the net irradiances above and below a cloud [Eq. (3)], as well as the TOA and surface CRE [Eq. (6c)], becomes clear. While the global TOA CRE can directly be derived from reflected radiances (Loeb et al., 2005), for example from the Clouds and the Earth's Radiant Energy System (CERES) on the Aqua and Terra satellites (Wielicki et al., 1996), the derivation of the surface CRE also requires the knowledge of atmospheric absorptance or transmittance. In the case of CERES, the required cloud properties are obtained from retrievals of the accompanying imager, the Moderate Resolution Imaging Spectroradiometer (MODIS) (Minnis et al., 2011). As stated in the previous section, this is accomplished through lookup tables which are based on 1D calculations and therefore do not provide H.

Recognizing the crucial significance of horizontal photon transport for obtaining an accurate surface CRE, Barker et al. (2012) and Illingworth et al. (2015) described the ambitious goal of using 3D radiative transport operationally in the European radiative budget experiment Earth Clouds, Aerosols and Radiation Explorer (EarthCARE). They tested their algorithm with A-Train data. As a metric for 3D effects, they employed the commonly used difference between 3D and IPA calculations (e.g., Scheirer and Macke, 2003). In a similar manner, Ham et al. (2014) calculated the effect of horizontal photon transport on cloud absorption, transmission, and reflected radiance. They found these three quantities to be correlated when stratifying their results by cloud type after spatial aggregation to at least 5 km.

Since the studies cited above pertained to EarthCARE and CERES, they only considered broadband effects. This does not allow distinguishing between A_λ and H_λ by means of their

[5] The cloud contribution term $CRE^{TOA} - CRE^{surface}$ also contains multiple scattering enhancements of gas absorption due to clouds (Kindel et al., 2011), which may lead to a considerable increase of the gas absorption (Schmidt and Pilewskie, 2012).

Atmos. Chem. Phys. Discuss., doi:10.5194/acp-2015-911, 2016
Manuscript under review for journal Atmos. Chem. Phys.
Published: 14 March 2016

Atmospheric Chemistry and Physics Discussions

distinct spectral characteristics. Our approach, first presented by Schmidt et al. (2014), bridges this gap. In this paper, we will focus exclusively on the near-ultraviolet and visible wavelength range and explore the spectral fingerprint from cloud inhomogeneities in conjunction with molecular scattering in H_λ, which also imprints itself on reflected radiances (Song et al., 2015). We chose to not include aerosols in either study, primarily to isolate the spectral signature of heterogeneous clouds before considering the more general case of clouds and aerosols in combination.

The spectral dependence of the horizontal photon transport across the full shortwave range will be published separately (Song, 2016). Our expectation for the future, discussed in the conclusions (Section 9), is that future energy budget studies will capitalize on the spectral fingerprint of cloud inhomogeneities and derive H by way of the associated spectral radiance perturbations.

3. Cloud Data

Our study builds upon the results by Schmidt et al. (2010) and therefore uses the same cloud case, a tropical convective core with anvil outflow, observed during the TC^4 experiment on 17 July 2007 (from 1519 to 1535 UTC) by the NASA ER-2 aircraft about 300 km south of Panama. Two realizations of the observed cloud field were used as input to 3D radiative transfer calculations, one based on airborne imagery only (as in the earlier study, Section 3.1), and one based on merged airborne and geostationary imagery (Section 3.2) to study large-scale effects.

3.1 Sub-scene from ER-2 passive and active remote sensors

Level-2 cloud retrievals of the Moderate Resolution Imaging Spectrometer (MODIS) Airborne Simulator (MAS: King et al., 1996; King et al., 2010) were combined with reflectivity profiles from the Cloud Radar System (CRS: Li et al., 2004) as described in detail by Schmidt et al. (2010). The primary information originates from MAS optical thickness, thermodynamic phase, effective radius, and cloud top height retrievals for each pixel (x,y) within the imager's swath (roughly 20 km for a cloud top height of 10 km). The imagery-derived information was extended into the vertical dimension z by simple approximations:

Atmos. Chem. Phys. Discuss., doi:10.5194/acp-2015-911, 2016
Manuscript under review for journal Atmos. Chem. Phys.
Published: 14 March 2016

Atmospheric Chemistry and Physics Discussions

(1) The effective radius from MAS, $r_e(x,y)$, was used throughout the vertical dimension z although representative only of the topmost layer. Since the study is limited to the near-ultraviolet and visible wavelength range where cloud absorption is negligible, this simplification only affects the scattering phase function. Approximating it with that at cloud top is acceptable because to first approximation, 3D radiative transfer is determined by the distribution of cloud extinction.

(2) The MAS retrieved optical thickness $\tau(x,y)$ for each pixel was vertically distributed by using the water content profile from CRS: $WC(z) = 0.137 \times Z^{0.64}$ (Liu and Illingworth, 2000) where Z is the radar reflectivity from CRS in dBZ. Since WC(z) is only available along the flight track, nadir-only CRS profiles were also used across the entire MAS swath (shifted vertically by z_0 to match the MAS cloud top height at off-nadir pixels). Cloud extinction β for each voxel (x,y,z) was thus obtained as

$$\beta(x,y,z) = \tau_{MAS}(x,y) \times WC(z+z_0) / \sum_z WC(z) \quad .$$

Along the flight track, the mismatch between MAS- and CRS-retrieved cloud top height is $\leqslant$ 0.5 km. The CRS-derived average cloud top height is 10.8 km, and the mean geometrical thickness is 3.3 km.

The resulting cloud field was gridded to a resolution of 0.5 km horizontally and 1.0 km vertically (chosen larger than the mismatch between CRS and MAS in cloud top height).

Figure 1 shows the cloud optical thickness field from MAS after regridding, with the nadir track highlighted as a dashed line. The length of this scene is 192 km (384 pixels in x), and the width is 17.5 km (35 pixels in y).

3.2 Large-scale field from ER-2 data merged with geostationary imagery

To generalize our findings to larger scales than 17.5 km, we embedded the sub-scene from the ER-2 remote sensors in the context of the large-scale cloud field as retrieved from the Geostationary Operational Environmental Satellite West (GOES-11). The imager onboard GOES-11 has five channels centered at 0.65, 3.9, 6.7, 10.7 and 12.0 μm. In the sampling region, cloud property retrievals were produced at 1515 and 1545 UTC (Walther and Heidinger, 2012),

Atmos. Chem. Phys. Discuss., doi:10.5194/acp-2015-911, 2016
Manuscript under review for journal Atmos. Chem. Phys.
Published: 14 March 2016

of which we chose the earlier one because it was more consistent with the MAS retrieval.

Figure 2 shows the extended cloud scene (240 km × 240 km). Outside the MAS swath, GOES-11 retrievals were used instead of those from MAS. Similarly, as for the sub-scene cloud, the effective radius retrieval was extended throughout the vertical dimension. The optical thickness was distributed vertically using the CRS profile with the closest match in column-integrated water path (as compared to the retrieved value from GOES) and adjusted in altitude to match the cloud top height retrievals from GOES-11. This approach for distributing profile information from active instrumentation across the swath of a passive imager is more simplistic than that developed by Barker et al. (2011) who used multi-spectral radiances from MODIS. Transferring radar information to off-nadir pixels as far away as 120 km is not necessarily justified due to spatial de-correlation of cloud systems (Miller et al., 2014). However, in the absence of any other information, it was considered the best alternative to estimating the cloud vertical structure without any *a priori* knowledge.

4. Model calculations

The calculations in this study were performed with the 3D Monte Carlo Atmospheric Radiative Transfer Simulator (MCARaTS: Iwabuchi, 2006). MCARaTS is an open-source code written in FORTRAN-90, which can be obtained at sites.google.com/site/mcarats/. It calculates shortwave and longwave spectral or broadband radiances and irradiances based on a forward propagating photon transport algorithm. It is optimized to run efficiently on parallel computers.

In addition to the two 3D cloud fields described in Section 3, the standard tropical summer atmosphere as distributed within the libRadtran radiative transfer package (www.libradtran.org: Mayer and Kylling, 2005) was used to prescribe the vertical profile of temperature, pressure, water vapor and other atmospheric gases. For gas molecular scattering, we calculated the optical thickness for each layer with the approximation by Bodhaine et al. (1999) and selected the Rayleigh scattering phase function from MCARaTS. For gas molecular absorption, we adopted the correlated *k*-distribution method described by Coddington et al. (2008). It was originally based on Mlawer and Clough (1997), modified for the shortwave by Bergstrom et al. (2003), and was specifically developed for the Solar Spectral Flux Radiometer

Atmos. Chem. Phys. Discuss., doi:10.5194/acp-2015-911, 2016
Manuscript under review for journal Atmos. Chem. Phys.
Published: 14 March 2016

Atmospheric Chemistry and Physics Discussions

(SSFR: Pilewskie et al., 2003). The SSFR instrument line shape (6-8 nm full-width half-maximum) defines the width of the channels in this study (narrower than MODIS or MAS channels). The spectrum by Kurucz (1992) served as the extraterrestrial solar spectrum.

Calculations were performed at eleven wavelengths ranging from the near ultraviolet to the very-near infrared (350, 400, 450, 500, 550, 600, 650, 700, 750, 800, 1000 nm) to capture the spectral dependence of horizontal photon transport over a wide range of molecular scattering. At 1000 nm, molecular scattering is negligible and water vapor absorption is small; cloud absorption is negligible for all wavelengths. For pixels dominated by ice clouds, the scattering phase function and single scattering albedo were used from the general habit mixture of the ice cloud bulk models developed by Baum et al. (2011) (parameterized by the effective radius). For liquid water clouds (minority of cloud pixels), single scattering albedo and asymmetry parameter from Mie calculations were used in conjunction with a Henyey-Greenstein phase function (which generally simplifies irradiance calculations). In this study, all calculations were performed for an ocean surface albedo (Coddington et al., 2010) and for a solar zenith angle of 35° for consistency with the earlier publication by Schmidt et al. (2010). The solar azimuth angle was 60° (northeast). This will be generalized in future work. For each wavelength, 10^{11} (10^{12}) photons were used for the sub-scene (large-scale) cloud field, respectively. MCARaTS was run in the forward irradiance mode with periodic boundary conditions. For each 3D model run, calculations were also performed using the independent pixel approximation (IPA) where horizontal photon transport is deactivated.

5. Relationship between cloud spatial structure, net horizontal photon transport, and its spectral dependence

This section discusses the relationship between spatial structure and spectrally dependent horizontal photon transport based on the small sub-scene. Since true absorption, A_λ, is negligible, H_λ is equal to V_λ, the vertical flux divergence of an inhomogeneous cloud layer as defined in Section 2, with $h_{top} \approx 13$ km and $h_{base} \approx 8$ km.

Table 1 shows the optical thickness and effective radius for the eight highlighted pixels from Fig. 1 along with H_0, the horizontal photon transport at λ= 500 nm, expressed in percent of

Atmos. Chem. Phys. Discuss., doi:10.5194/acp-2015-911, 2016
Manuscript under review for journal Atmos. Chem. Phys.
Published: 14 March 2016

Atmospheric Chemistry and Physics Discussions

the incident irradiance. Positive values of H_0 are related to net photon loss to other pixels ("radiation donors"), negative values to net photon gain ("radiation recipient" pixels). In the small domain, values as high as 50% and as low as –125% were attained. H_0 cannot exceed 100%, but may go below –100%, in which case the radiation received through the sides of a column or voxel exceeds that from the top of the domain. Table 1 is sorted by H_0 rather than by optical thickness. It shows immediately that there is no relationship between the optical thickness (or cloud reflectance) and horizontal photon transport. For example, pixel #6 is a "radiation donor", whereas pixel #4 with roughly the same optical thickness is a recipient. For the extreme case of zero cloud optical thickness, the effect of horizontal photon transport had previously been observed as clear-sky radiance enhancement in the vicinity of clouds (Wen et al., 2007; Várnai and Marshak, 2009). Statistically, this enhancement is a function of the distance of a pixel to the nearest cloud. However, the horizontal scale of this dependence varies with the spatial context. Consequently, the distance to a certain cloud element cannot generally be used to parameterize 3D cloud effects for individual pixels, whether cloud-free or cloud-covered. This is illustrated when considering pixels #4-#8 in the anvil outflow, which have low optical thickness (around 10) compared to the convective core (optical thickness ≥ 40) overflown from 15.45-15.48 UTC. The small contrasts in optical thickness (reflectance) between the pixels in close proximity tend to drive the sign of H_0 to a greater extent than the exchange of radiation with the (bright) core (for example, #6→#7, #5→#4, #7→#8, but not #5→#6). On the other hand, pixels #2 and #3 have relatively low values of H_0 although they have the largest optical thickness of all eight pixels. While still donors, the magnitude of net horizontal flux to other pixels seems to be diminished by the vicinity to the convective core. Overall, the direction, let alone the magnitude of net horizontal flux, is difficult to predict from the distribution of optical thickness, emphasizing 3D effects as a non-local phenomenon.

For the highlighted pixels in Table 1 (#5-#8), Figs. 3a shows the spectral shape of H_λ. The absolute value H_λ increases with wavelength until it reaches an asymptotic value towards near-infrared wavelengths, which we denote Δ_∞. Donor pixels ($H_\lambda > 0$) are associated with a positive spectral slope, $S_\lambda \equiv dH_\lambda / d\lambda > 0$; recipient pixels have a negative spectral slope. Remote sensing

Atmos. Chem. Phys. Discuss., doi:10.5194/acp-2015-911, 2016
Manuscript under review for journal Atmos. Chem. Phys.
Published: 14 March 2016

Atmospheric Chemistry and Physics Discussions

studies (e.g., Marshak et al., 2008; Várnai and Marshak, 2009) had previously established that the above mentioned *radiance enhancement* for clear-sky pixels near clouds was associated with "apparent bluing", and proposed molecular scattering as the underlying cause for this spectral dependence. To demonstrate that the same effect is at work here, molecular scattering was deactivated in MCARaTS, keeping everything else the same in the calculations. In the resulting spectra (* symbols in Fig. 3a), the wavelength dependence in the near-ultraviolet and visible range disappears almost entirely, suggesting molecular scattering as the primary cause for the spectral shape not only for clear-sky, but also for cloudy pixels. This begs the question (addressed in the next section) of how it is possible to observe such a significant spectral effect for cloudy pixels, given that cloud scattering outweighs molecular scattering by far. After turning molecular scattering off, the remaining variability in H_λ is due to the weak dependence of cloud scattering properties on wavelength and droplet or crystal effective radius, as well as minor gas absorption features.

To first order, the spectral shape over the range of 350 to 650 nm can be characterized by a single number—the spectral slope at λ = 500 nm, S_0 (obtained from a linear fit to $H_{\lambda=350\text{-}600\ \text{nm}}$). Table 1 lists the value of S_0 for the eight pixels from Fig. 1, whereas Fig. 3b depicts the relationship between H_0 and S_0 for *every* pixel. It shows that not only the sign, but also the magnitude of the net horizontal photon transport, is surprisingly well correlated with its slope at 500 nm (in %/100 nm). This suggests that the phenomenon observed by Schmidt et al. (2010) for a few isolated data points is a general occurrence throughout a heterogeneous cloud field. The close relationship between the magnitude and spectral shape of net horizontal photon transport is the basis for the spectral parameterization of H_λ, developed in the next section.

In H_0–S_0 space, all IPA calculations (red dots in Fig. 3b) are reduced to the origin because they do not allow pixel-to-pixel radiation exchange by definition. Owing to periodic boundary conditions, the cloud domain average of H is zero. The calculations without molecular scattering (grey dots) confirm that molecular scattering dominates the spectral shape throughout the domain. The vertical spread of the grey data points is due to the other factors mentioned above (e.g., variability in cloud microphysics). To some extent, it is also apparent in the IPA calculations.

Atmos. Chem. Phys. Discuss., doi:10.5194/acp-2015-911, 2016
Manuscript under review for journal Atmos. Chem. Phys.
Published: 14 March 2016

Atmospheric Chemistry and Physics Discussions

6. Physical mechanism and parameterization

Our interpretation of Fig. 3 is that H_λ can be understood as the combination of two terms:

$$H_\lambda = H_\infty + \delta(\lambda). \quad (7)$$

1. The constant offset H_∞ is caused by column-to-column radiation exchange between cloud elements. This is illustrated by Fig. 4 that shows the vertical profile of (a) downwelling, (b) net, and (c) upwelling irradiance at 1000 nm wavelength for the cloud field from Fig. 1. A change of net irradiance between altitudes z_0 and z_1 corresponds to net radiation loss or gain within that layer. In this case, the domain-averaged profile of net irradiance (black line in Fig. 4b) decreases slightly near the surface, due to small absorption in the wing of the 936 nm water vapor band[6]. When subsampling over columns with a cloud optical thickness $\tau < 1$, or $\tau > 120$, the 3D calculations differ from the IPA calculations because column-to-column radiation transfer is enabled. Above the cloud field, columns with high cloud optical thickness have higher reflectance than the domain average (Fig. 4c) and collectively lose radiation to those with lower optical thickness; the opposite is true below the cloud where columns with high optical thickness have lower transmittance (Fig. 4a). The magnitude of the net horizontal photon transport (the difference of net irradiances at the bottom and top altitude of a layer) increases with the geometrical layer thickness. Fig. 5 conceptually depicts the processes at work. Above clouds, net horizontal photon transport (reflected radiance, projected into a horizontal plane) occurs from the high- to low-reflectance column. Below clouds, the direction is reversed because the transmittance of thin clouds is larger than that of thicker clouds.[7] This simplified figure should *not* be interpreted to suggest that the net horizontal transport generally occurs along gradients of cloud optical thickness. As stated

[6] Alternative choices would be 860 nm (although with non-negligible molecular scattering) or 1040 nm (with small cloud absorption under certain conditions, see LeBlanc et al. (2015)).

[7] Note that below $\tau \approx 4$, directly transmitted radiation dominates the downwelling irradiance, and the cloud may not act as a "diffuser" as shown in Fig. 5. The direction of the green arrows is then along the direct beam.

Atmos. Chem. Phys. Discuss., doi:10.5194/acp-2015-911, 2016
Manuscript under review for journal Atmos. Chem. Phys.
Published: 14 March 2016

Atmospheric Chemistry and Physics Discussions

above, its direction and magnitude depends not only on directly adjacent columns, but also on the large-scale context, which is why a parameterization of 3D cloud effects in clear-sky areas in terms of the distance to the nearest cloud is only possible in a statistical way, but not on an individual pixel basis (Wen et al., 2007). The value of H_∞ can be obtained from H_λ for wavelengths where molecular scattering becomes negligible and where cloud and gas absorption are small compared to H_λ: $A_\lambda \ll H_\lambda$. For the purpose of this study, we chose λ = 1000 nm: $H_\infty \approx H_{\lambda=1000\ \mathrm{nm}}$.

2. The spectral perturbation δ_λ, superimposed on H_∞, introduces the wavelength dependence of H_λ. It is perhaps not immediately intuitive why molecular scattering would reduce the magnitude of H_λ as indicated by the symbolic blue arrows in Fig. 5. Molecular scattering essentially reduces the directionality of horizontal photon transport by redistributing radiation, part of which can then be detected as enhanced clear-sky reflectance of clouds (Marshak et al., 2008). A different, secondary process occurs when radiation is scattered out of the direct beam in clear-sky areas into cloud shadows (dashed blue arrow in Fig. 5). It is spectrally dependent as δ_λ but, unlike δ_λ, *independent* of H_∞ and its direction—thus increasing the net radiation under both optically thick and thin clouds. For 550 nm wavelength and shorter (not shown in Figure 4), the net irradiance does indeed increase towards the surface, both for $\tau > 120$ and for $\tau < 1$. This secondary effect is not explicitly captured by the first-order parameterization given below.

We express the proportionality of δ_λ to H_∞ as

$$\delta(\lambda) = -\varepsilon\left(\frac{\lambda}{\lambda_0}\right)^{-x} H_\infty \qquad (\varepsilon \geq 0,\ \lambda_0 = 500\ \mathrm{nm}), \tag{8}$$

where $(\lambda/\lambda_0)^{-x}$ describes the wavelength dependence, and ε is the constant of proportionality. The layer thickness for which H_λ is derived affects both H_∞ and δ_λ, but only marginally changes the correlation *between* them. Therefore, ε is a general parameter that can be used for relating spatial inhomogeneities and spectral signature of a cloud scene as a whole. It depends on scene parameters such as surface albedo, solar zenith angle, and cloud micro- and macrophysics (including vertical structure). This dependence and the secondary effect due to molecular

Atmos. Chem. Phys. Discuss., doi:10.5194/acp-2015-911, 2016
Manuscript under review for journal Atmos. Chem. Phys.
Published: 14 March 2016

Atmospheric Chemistry and Physics Discussions

scattering mentioned above will be explored in a follow-on publication (Song, 2016). Using Eq. (8), the spectral slope S_0 from the previous section can then be derived as

$$S_0 = \left.\frac{dH_\lambda}{d\lambda}\right|_{\lambda=\lambda_0} = \left.\frac{d\delta(\lambda)}{d\lambda}\right|_{\lambda=\lambda_0} = x\varepsilon\frac{H_\infty}{\lambda_0}, \quad (9)$$

By combining Eqs. (7) and (8), one obtains $H_0 = H_{\lambda=500\ \mathrm{nm}} = H_\infty(1-\varepsilon)$, and Eq. (9) can be rewritten as

$$S_0 = \frac{x\varepsilon}{1-\varepsilon}\frac{H_0}{\lambda_0}, \quad (10)$$

where $x\varepsilon/(1-\varepsilon)\lambda_0$ is the slope of the linear regression derived using all pixels in the cloud domain (for example, Fig. 3b). Alternatively, one can derive both ε and x for each individual pixel from the regression of

$$\log\left(-\frac{\delta(\lambda)}{H_\infty}\right) = \log\varepsilon - x\log\frac{\lambda}{\lambda_0} \quad (11)$$

with $\log\varepsilon$ as the intercept and x as the slope, as shown in Fig. 6a. In this example, the fit parameter is about 4 as would be expected if molecular scattering is the underlying physical mechanism. The two-dimensional PDF $p(x,\varepsilon)$ for the population of pixels in the domain peaks at $\{x,\varepsilon\} \approx \{3.85, 0.065\}$ but has a considerable spread in both parameters, which is caused by pixels with negligible horizontal photon transport (and consequently large uncertainties in the fit parameters). The dashed lines in Fig. 3a show the fitted spectra (labeled "theoretical") from this approach. For practical purposes, we fix $x \equiv 4$ for the remainder of this paper. This allows using

$$H_\lambda = H_\infty\left(1-\varepsilon\left(\frac{\lambda}{\lambda_0}\right)^{-4}\right) \quad (12)$$

instead of Eq. (11) and derive ε and H_∞ for each pixel from a linear regression of H_λ versus $(\lambda/\lambda_0)^{-4}$ (i.e., H_∞ is no longer a required input parameter as for the logarithmic regression). With

Atmos. Chem. Phys. Discuss., doi:10.5194/acp-2015-911, 2016
Manuscript under review for journal Atmos. Chem. Phys.
Published: 14 March 2016

Atmospheric Chemistry and Physics Discussions

ε known, S_0 can be calculated from Eq. (9)[8], and a domain-wide "effective" ε can be derived from the slope of the regression line of S_0 versus H_∞ for all pixels (Eq. (10) with $x = 4$). Fig. 7 shows the distribution of ε as derived from (12) for all those pixels with $\Delta(\varepsilon) < 5\%$. The median of this distribution (0.069) is almost identical to the "effective" value of ε (0.067). The standard deviation of the distribution is about 0.01. This means that the parameterized correlation between net horizontal transport and its spectral dependence can be applied to the domain as a whole as well as for individual pixels; if the spectral shape of H_λ is known, one can infer its magnitude throughout the near-ultraviolet and visible wavelength range. The correlation is robust regardless of the cloud context of a pixel, which is remarkable given the considerable variability in distance-based measures of 3D cloud effects (Várnai and Marshak, 2009).

Although our study was instigated by aircraft measurements, its findings are also relevant for satellite-based derivations of cloud radiative effects since the spectral perturbations δ_λ propagate into observed radiances and imprint a spectral signature of H_λ (Song et al., 2015). In this context, it is important to emphasize the fundamental difference between radiance and irradiance and their observation from space and aircraft, respectively. Radiances are mainly affected by radiative smoothing and roughening within a cloud layer (e.g., Marshak et al., 2006). In addition, aircraft measurements also exhibit geometrical smoothing in their power spectra (Schmidt et al., 2007a), especially when acquired high above a cloud field. For this reason, radiance-derived cloud albedo products such as from aircraft imagers (Schmidt et al., 2007b; Kindel et al., 2010) often do not match their measured counterparts. Through our study, we now understand why this mismatch [Fig. 7 in Kindel et al., 2010) is associated with a spectral inconsistency in the albedo spectra (Schmidt and Pilewskie, 2012)—it can simply be explained by the term δ_λ in Eq. (7).

In principle, the mean albedo of an inhomogeneous cloud field derived from CERES

[8] This is more accurate than derivation of the slope from a linear fit to the spectrum as used for Fig. 3, which, due to the non-linearity of the spectral dependence, differs from that of the tangent if finite wavelength intervals are used.

Atmos. Chem. Phys. Discuss., doi:10.5194/acp-2015-911, 2016
Manuscript under review for journal Atmos. Chem. Phys.
Published: 14 March 2016

Atmospheric Chemistry and Physics Discussions

observations should be fairly insensitive to 3D effects because they are folded into empirical anisotropy models of such scene types.[9] By contrast, surface cloud radiative effects are much less constrained by direct CERES observations because cloud transmittance has to be derived from concomitant imagery. This is where biases introduced by H_λ are most significant. For the remainder of this paper, we therefore analyze the significance of H for varying degrees of spatial aggregation (Section 7), and make the connection to cloud transmittance (Section 8).

7. Scale dependence and spatial aggregation

The results presented so far (e.g., in Fig. 3b) are based on calculations at a resolution of 0.5 km. The question is whether the correlation between the magnitude and spectral shape of H is scale invariant, and to what extent the effect of horizontal photon transport can be mitigated by spatial aggregation. To answer this question, we successively coarsened the pixel resolution to 15 km, the largest super-pixel contained within the MAS swath (Fig. 1). Figure 8a shows that the correlation is indeed independent of the spatial aggregation scale and thus pixel size. The magnitude of H_0 decreases with pixel size: it ranges from +6% to –5% at 15 km resolution (close to CERES for nadir viewing), compared to about ±50% at 1-5 km (resolution of various MODIS level-2 products). Eq. (1) suggests that neglecting horizontal photon transport will cause biases in pixel-level products such as cloud transmittance and surface insolation. In the next section, we will examine to what extent horizontal photon transport translates into 3D-1D transmittance biases. Here, we use the large cloud scene (Fig. 2) to estimate for which aggregation scale beyond 15 km the magnitude of H_0 drops below the radiometric uncertainty of typical space- or ground-based radiometers (3-5%), at which point 3D cloud effects become insignificant from a radiative energy budget point-of-view.

The results for the large scene, shown in Fig. 8b, confirm that the correlation is preserved for scales up to 70 km. However, H_0 at 15 km resolution varies from +17% to –13% throughout

[9] This is only true if the empirical anisotropy models adequately accomplish the radiance-to-irradiance conversion.

Atmos. Chem. Phys. Discuss., doi:10.5194/acp-2015-911, 2016
Manuscript under review for journal Atmos. Chem. Phys.
Published: 14 March 2016

Atmospheric Chemistry and Physics Discussions

the large scene domain, much more than in the MAS-only domain (+6% to –5%). One explanation for this larger range is the greater complexity of the large domain, providing a more extensive sample of cloud variability than the smaller sub-scene. This becomes quite clear when looking at the spatial distribution of horizontal photon transport: In Fig. 8c, we chose to plot S_0 (y-axis in Fig. 8b) rather than H_0. They are practically interchangeable thanks to the correlation between the two. The distribution of effective donor, recipient, and neutral regions (red, blue, green, respectively) bears almost no resemblance to the optical thickness field from Fig. 2. This demonstrates once again that horizontal photon transport cannot be derived from the spatial distribution of clouds in any simple way; strong contrasts between negative and positive H_0 (or S_0) can arise in optically thin boundary layer clouds (southwest corner of Fig. 2 and 8c) as well as in optically thick areas (deep convection, northeast corner of cloud scene). Extracting the GOES-MAS large-scene results within the boundaries of the small MAS-only scene (marked by the green rectangle in Fig. 8c) allows estimating the large-scale exchange of the small domain with its context. The average value of H_0 within the small-scene subset is +7.9%, which means that the small scene effectively loses photons to its surroundings. This would not be detectable for such a large aggregation scale (where the entire MAS domain represents a single "super-pixel"). This net energy export is not reproduced by the calculations based on the MAS-only domain where the mean value of H_0 is zero, in keeping with energy conservation (satisfied by periodic boundary conditions in the radiative transfer model). The range of H_0 in the MAS-only sub-scene of the GOES-MAS scene is +17% to –6% at 15 km aggregation scale. This is still a larger range than obtained from the MAS-only calculations (+6% to –5%), even after sub-setting the results from the large scene to the boundaries of the small ones. The reason is simply that 15 km super-pixel size is already half the width of the MAS-only domain. Boundary conditions enforce the convergence of H_0 to zero as the area ratio of pixel to domain size approaches 1, which causes an underestimation of the variability of H_0 for large aggregation scales. By contrast, photons can also travel outside the confines of the domain in the real world as represented by the larger GOES-MAS cloud scene in our study.

This is illustrated in Figure 8d, which shows the range of H_0 for both the large and the

Atmos. Chem. Phys. Discuss., doi:10.5194/acp-2015-911, 2016
Manuscript under review for journal Atmos. Chem. Phys.
Published: 14 March 2016

Atmospheric Chemistry and Physics Discussions

small cloud scene as a function of aggregation scale. At small scales, the range is comparable for the small and large scene. At 15 km aggregation scale, the range obtained from the small scene has decreased to about half that of the large one. At 50 km pixel resolution, H_0 ranges from +7% to –3% (+5% to –1% at 70 km). It is likely that the boundary conditions imposed on the large domain also cause an underestimation of the H_0 variability at these large scales. Nevertheless, these results suggest that above 60 km super-pixel size (about 3 × 3 CERES nadir footprints), horizontal photon transport can be neglected for this cloud scene, based on a 3% uncertainty threshold. This is only true when aggregating all native-resolution pixels, regardless of whether they are flagged as clear sky or as cloud-covered. However, sampling cloudy and clear pixels *separately* would result in much larger biases than 3% because high optical thickness pixels are more likely to be effective photon donors than low-optical thickness or clear pixels, causing an asymmetry in the distribution of H_0 (Song et al., 2015).

8. Significance for Cloud Radiative Effect

In this section, we evaluate the ramifications of net horizontal photon transport on estimates of cloud radiative effects. For any atmospheric column, H is connected to R and T through Eq. (1) and manifests itself in a transmittance and reflectance bias:

$$\Delta T = T^{IPA} - T^{3D} \tag{13a}$$

$$\Delta R = R^{IPA} - R^{3D}. \tag{13a}$$

Juxtaposing energy conservation for a horizontally homogeneous atmosphere ($T^{IPA} + R^{IPA} = 1$) with Eq. (1) for conservative scattering ($T^{3D} + R^{3D} = 1 - H$) yields the plausible relationship

$$H = \Delta T + \Delta R, \tag{14}$$

which means that the error introduced by horizontal photon transport is partitioned into transmittance and reflectance bias. Since the bias ΔR is folded into the empirical radiance-to-irradiance conversion employed by CERES, we focus on ΔT in this study.

For the eight super-pixels #11–#18 from Fig. 2, Fig. 9a shows the IPA bias ΔT, ranging from +2% to +14% in the mid-visible. Its spectral dependence is more complicated than the one shown for H in Fig. 3a, with a less obvious correlation between magnitude and spectral shape.

Atmos. Chem. Phys. Discuss., doi:10.5194/acp-2015-911, 2016
Manuscript under review for journal Atmos. Chem. Phys.
Published: 14 March 2016

Atmospheric Chemistry and Physics Discussions

Nevertheless, Fig. 9b shows a remarkable correlation between H_0 and ΔT_0 ($T^{\mathrm{IPA}} - T^{\mathrm{3D}}$ at 500 nm) for the same aggregation scales as in Fig. 8b. For example, the H_0 range of +15% to –10% translates into +19% to –12% in ΔT_0 for a horizontal resolution of 20 km. Linear regression between H_0 and ΔT_0 suggests that in this case, H_0 propagates mainly into ΔT_0, whereas it is uncorrelated with ΔR_0 for scales below 20 km (Fig. 10).

For simplicity, the spectral dependence of ΔT as shown in Fig. 9a is approximated by

$$\Delta T_\lambda = T_\lambda^{IPA} - T_\lambda^{3D} = \xi_0\big|_{350-600nm} \times (\lambda - \lambda_0) + (T_0^{IPA} - T_0^{3D})\ ;\ \lambda_0 = 500\ \mathrm{nm} \qquad (15)$$

where ξ_0 is the spectral slope of $T_\lambda^{IPA} - T_\lambda^{3D}$ calculated from the spectrum between 350 and 600 nm. Fig. 9c shows that the spectral slopes of H and ΔT, S_0 and ξ_0, are correlated despite the more complicated spectral dependence of T compared to that of H (Fig. 9a). However, there is clearly no 1:1 relationship as found between H_0 and ΔT_0 above. For example, S_0 = –10%/100 nm corresponds to only ξ_0 = –6%/100 nm. This changes when extending the vertical layer boundaries (8-13 km so far, bracketing only the cloud layer itself) to the atmosphere reaching from the ground to cloud top. This distinction is indicated by hats above all quantities. This is slightly different from the definition of $\hat{T}$ in Section 2 where the upper boundary is the top of atmosphere, not the top of the cloud. Fig. 9d not only shows a much stronger spectral dependence of $\Delta\hat{T}$ (surpassing that of $\hat{H}$) compared to that of ΔT and H in Fig. 9c, but that the correlation is no longer scale invariant. This means that the vertical bracket for deriving T, R, and H has to be chosen with consideration of the vertical location of the cloud layer. By contrast, the correlation between H and S as discussed in Section 6 is fairly independent of the layer boundaries.

For future studies of IPA-3D biases in satellite-derived estimates of surface cloud radiative effects, Fig. 4b suggests the center of a cloud as upper boundary of the bracket where $\left|dF_{net}/dz\right|$ reaches a domain-wide minimum because 3D effects can be vertically separated into a transmittance and reflectance part below and above this level, respectively. Moreover, the correlation between ΔT and its spectral dependence ξ_0 (not shown) can be exploited to detect IPA-3D biases in ground-based irradiance measurements below cloud fields (Song, 2016). While our study suggests that horizontal photon transport mainly propagates into transmittance biases, there is some indication (Fig. 10) that at scales above 20 km, non-zero values of H_0 translate into

Atmos. Chem. Phys. Discuss., doi:10.5194/acp-2015-911, 2016
Manuscript under review for journal Atmos. Chem. Phys.
Published: 14 March 2016

Atmospheric Chemistry and Physics Discussions

albedo (reflected irradiance) biases as well. This increasing correlation with scale is probably associated with the gradual de-correlation between $\hat{S}_0$ and $\hat{\xi}_0$ observed in Fig. 9b. In order to improve satellite-based estimates of cloud radiative effects, it is important to understand how H_0 is partitioned into ΔT and ΔR [Eq. (14)] at different aggregation scales. A detailed study would need to be conducted for different cloud morphologies, sun angles and surface albedos and is left for the future. Meanwhile, Song et al. (2015) investigate the link between net horizontal transport in cloud fields and spectral perturbations in reflected *radiance*.

9. Summary and conclusions

Deriving the radiative effects of inhomogeneous cloud scenes from observations by satellite, aircraft, or at the surface is often portrayed as an intractable problem because it cannot be accomplished by isolating a pixel from its spatial context. At the core of the issue is pixel-to-pixel exchange of radiation, or net horizontal photon transport, which occurs over a range of scales. The original motivation for this study was to gain a physical understanding of this phenomenon's spectral dependence in the near-ultraviolet and visible wavelength range, which had been found in aircraft irradiance observations (Schmidt et al., 2010). We were able to identify molecular scattering as the underlying mechanism for the spectral dependence using three-dimensional radiative transfer calculations with cloud imagery and radar observations as input. When de-activating molecular scattering in the radiative transfer model, the wavelength dependence disappeared almost entirely in the vertical flux divergence V, which comprises net horizontal flux density H as well as true layer absorption A. To simplify the analysis, we limited our study to conservative scattering by choosing wavelengths with negligible gas or cloud absorption ($A \approx 0$), and by excluding aerosols. When activated in the model, molecular scattering manifested itself as a spectral perturbation (more accurately: modulation) δ_λ to an otherwise *spectrally neutral* horizontal flux density H_∞, which in turn could be traced back to horizontal exchange of radiation due to spatial inhomogeneity of cloud elements within the domain. Beyond the original scope of this study, we made a few surprising discoveries:

1. The spectral perturbation δ_λ is not independent of the spectrally neutral part H_∞ caused by the clouds themselves. Instead, the mid-visible spectral slope of H_λ is correlated with H itself

Atmos. Chem. Phys. Discuss., doi:10.5194/acp-2015-911, 2016
Manuscript under review for journal Atmos. Chem. Phys.
Published: 14 March 2016

Atmospheric Chemistry and Physics Discussions

(i.e., with the magnitude of the spectrally neutral part H_∞), which led to the simple parameterization

$$\delta_\lambda = -\varepsilon\left(\frac{\lambda}{\lambda_0}\right)^{-x} H_\infty .$$

2. We were able to show that the exponent x is close to 4, which further confirmed molecular scattering as the dominating physical mechanism behind the spectral perturbation. The constant of proportionality, ε, can be regarded as universally valid for all pixels within the cloud domain, independently of the vertical or horizontal spatial distribution of clouds. This means that the spectrally dependent horizontal photon transport can be represented as

$$H_\lambda = H_\infty + \delta_\lambda = H_\infty\left(1 - \varepsilon\left(\frac{\lambda}{\lambda_0}\right)^{-4}\right)$$

for *each pixel* within the domain with $\varepsilon = 0.7 \pm 0.1$. It seems remarkable that one single value of ε should suffice to describe the relationship between the magnitude of H (caused by clouds) and its spectral dependence (imprinted on H by a completely different physical process, molecular scattering) – especially considering the range of different clouds within the domain. The correlation holds for each pixel, no matter what its spatial context may be. Once ε is established for a given cloud scene, the spectral perturbations associated with horizontal photon transport can be derived for each pixel if the value of H is known. Conversely, if the spectral shape of H is known, the value of H can easily be inferred. This may be especially significant considering that H cannot be directly observed from space. It is likely that the spectral perturbations will propagate into the observed radiances. Indeed, Song et al. (2015) found evidence of this connection in aircraft data. In fact, Várnai and Marshak (2009) previously reported this effect in clear-sky radiance observations near clouds. The close correlation that we found in our study may be a pathway to inferring the magnitude of H from its spectral manifestation in the observed radiances.

3. The correlation and parameterization hold for a range of spatial aggregation scales, and are fairly independent of the location of the bracketing altitudes that define the layer. This scale

Atmos. Chem. Phys. Discuss., doi:10.5194/acp-2015-911, 2016
Manuscript under review for journal Atmos. Chem. Phys.
Published: 14 March 2016

invariance only breaks down when extending a layer very close to the surface where a secondary spectral effect has to be factored in (see Section 6 and dashed arrow in Figure 5).

4. The observed correlation between H and its spectral shape can also be found between transmitted irradiance T and its spectral shape, although it is not scale invariant beyond 20 km.
5. H is correlated with ΔT, the IPA bias for each pixel, but not ΔR (at least at small scales). This means that 3D cloud effects in the form of horizontal photon transport translate almost exclusively into a transmittance bias. At scales above 20 km, a correlation between H and ΔR does emerge, which requires further study. The correlation between H and ΔT can potentially be exploited for ground-based spectral irradiance observations (Song, 2016).

Few of these findings could be expected at the outset of our research, and they evoke a number of new questions:

1. How does the discovered correlation and the constant of proportionality in its parameterization, ε, depend on scene parameters such as solar zenith and azimuth angle, surface albedo (magnitude and spectral dependence), and cloud morphology and microphysics? What "drives" the parameter ε?
2. Can the spectral perturbations associated with H indeed be detected in reflected radiances, and can they be used to infer the magnitude of H indirectly?
3. Can the findings for the near ultraviolet and visible wavelength range be generalized to the near-infrared wavelength range where clouds and atmospheric gases do absorb?
4. What are the implications of our findings for estimating aerosol radiative effects (such as heating rates) in presence of inhomogeneous cloud fields?
5. Can the method by Ackerman and Cox (1981) to correct for horizontal photon transport in aircraft measurements of atmospheric absorption by using a visible channel as basis for the correction of near-infrared absorption be upheld for future measurements, even in its modified form proposed by Kassianov and Kogan (2002)?
6. Can H and ΔT be derived from spectral perturbations in transmitted irradiance observations by ground-based spectrometers?

Atmos. Chem. Phys. Discuss., doi:10.5194/acp-2015-911, 2016
Manuscript under review for journal Atmos. Chem. Phys.
Published: 14 March 2016

Atmospheric Chemistry and Physics Discussions

Question 2 will be partially addressed by Song et al. (2015); questions 1, 3, 5, and 6 are discussed by Song (2016) and will be further investigated in future publications. Furthermore, questions 3 and 4 are subject of active research in the framework of an ongoing or planned field missions (NASA ORACLES and NSF ONFIRE, dedicated to the radiative effects and remote sensing of aerosol in vicinity to clouds). This publication constitutes a further contribution to the emerging field of cloud-aerosol spectroscopy (Schmidt and Pilewskie, 2012), which is expected to improve the estimation of cloud-aerosol parameters and their radiative effects through spectrally resolved observations from the ground, aircraft, and, ultimately, space.

Acknowledgements

The research presented in this paper was supported by NASA grant NNX14AP72G ("Linking the Radiative Energy Budget and Remote Sensing of Cloud and Aerosol Fields") within the radiation sciences program. The calculations were performed on the supercomputer "Janus", which is supported by the National Science Foundation (award number CNS-0821794) and the University of Colorado Boulder. It is a joint effort of the University of Colorado Boulder, the University of Colorado Denver, and the National Center for Atmospheric Research. Janus is operated by the University of Colorado Boulder.

Atmos. Chem. Phys. Discuss., doi:10.5194/acp-2015-911, 2016
Manuscript under review for journal Atmos. Chem. Phys.
Published: 14 March 2016

References

Ackerman, S. A., and Cox, S. K.: Aircraft observations of shortwave fractional absorptance of non-homogeneous clouds, J. Appl. Meteorol., 20, 1510-1515, 1981.

Arking, A.: The influence of clouds and water vapor on atmospheric absorption, Geophys. Res. Lett., 26, 2729-2732, 1981.

Barker, H. W., Jerg, M. P., Wehr, T., Kato, S.: Donovan D. P., and Hogan R. J.: A 3D cloud-construction algorithm for the EarthCARE satellite mission. Q. J. Roy. Meteorol. Soc., 137, 1042-1058, 2011.

Barker, H. W., Kato, S., and Wehr, T.: Computation of solar radiative fluxes by 1D and 3D methods using cloudy atmospheres inferred from A-train satellite data, Surv. Geophys., 33, 657–676, 2012.

Baum, B. A., Yang, P., Heymsfield, A. J., Schmitt, C., Xie, Y., Bansemer, A., Hu, Y. X., and Zhang, Z.: Improvements to shortwave bulk scattering and absorption models for the remote sensing of ice clouds. J. Appl. Meteor. Climatol., 50, 1037-1056, 2011.

Bergstrom, R. W., Pilewskie, P., Schmid, B., and Russell, P. B.: Estimates of the spectral aerosol single scattering albedo and aerosol radiative effects during SAFARI 2000, J. Geophys. Res., 108, 8474, doi:10.1029/2002JD002435, 2003.

Bodhaine, B. A., Wood, N. B., Dutton, E. G., and Slusser, J. R.: On Rayleigh optical depth calculations, J. Atmos. and Ocean. Tech., 16, 1854-1861, 1999.

Coddington, O., Schmidt, K. S., Pilewskie, P., Gore, W. J., Bergstrom, R. W., Roman, M., Redemann, J., Russell, P. B., Liu, J., and Schaaf, C. C.: Aircraft measurements of spectral surface albedo and its consistency with ground-based and space-borne observations, J. Geophys. Res., 113, D17209, doi:10.1029/2008JD010089, 2008.

Coddington, O. M., Pilewskie, P., Redemann, J., Platnick, S., Russell, P. B., Schmidt, K. S., Gore, W. J., Livingston, J., Wind, G., and Vukicevic, T.: Examining the impact of overlying aerosols on the retrieval of cloud optical properties from passive remote sensing, J. Geophys. Res., 115, D10211, doi:10.1029/2009JD012829, 2010.

Fritz, S., and MacDonald, T. H.: Measurements of absorption of solar radiation by clouds, Bull.

Am. Meteorol. Soc., 32, 205-209, 1951.

Ham, S.-H., Kato, S., Barker, H. W., Rose, F. G., and Sun-Mack, S.: Effects of 3-D clouds on atmospheric transmission of solar radiation: Cloud type dependencies inferred from A-train satellite data, J. Geophys. Res., 119, 943-963, 2014.

Illingworth, A. J., Barker, H. W., Beljaars, A., Ceccaldi, M., Chepfer, H., Clerbaux, N., Cole, J., Delanoë, J., Domenech, C., Donovan, D. P., Fukuda, S., Hirakata, M., Hogan, R. J., Huenerbein, A., Kollias, P., Kubota, T., Nakajima, T., Nakajima, T. Y., Nishizawa, T., Ohno, Y., Okamoto, H., Oki, R., Sato, K., Satoh, M., Shephard, M. W., Velázquez-Blázquez, A., Wandinger, U., Wehr, T., and van Zadelhoff, G.-J.: The EarthCARE Satellite: The Next Step Forward in Global Measurements of Clouds, Aerosols, Precipitation, and Radiation. Bull. Amer. Meteor. Soc., 96, 1311–1332, doi: http://dx.doi.org/10.1175/BAMS-D-12-00227.1, 2015.

Iwabuchi, H.: Efficient Monte Carlo methods for radiative transfer modeling. J Atmos. Sci., 63, 2324-2339, 2006.

Kassianov, E. I., and Kogan, Y. L.: Spectral dependence of radiative horizontal transport in stratocumulus clouds and its effect on near-IR absorption, J. Geophys. Res., 107(D23), 4712, doi:10.1029/2002JD002103, 2002.

Kato, S., Loeb, N. G., Rose, F. G., Doelling, D. R., Rutan, D. A., Caldwell, T. E., Yu, L., and Weller, R. A.: Surface irradiances consistent with CERES-derived top-of-atmosphere shortwave and longwave irradiances, J. Clim., 26, 2719-2740, 2013.

Kindel, B. C., Schmidt, K. S., Pilewskie, P., Baum, B. A., Yang, P., and Platnick, S.: Observations and modeling of ice cloud shortwave spectral albedo during the Tropical Composition, Cloud and Climate Coupling Experiment (TC^4), J. Geophys. Res., 115, D00J18, doi:10.1029/2009JD013127, 2010.

Kindel, B. C., Pilewskie, P., Schmidt, K. S., Coddington, O. M., and King, M. D.: Solar spectral absorption by marine stratus clouds: Measurements and modeling, J. Geophys. Res., 116, D10203, doi:10.1029/2010JD015071, 2011.

King, M. D., Menzel, W. P., Grant, P. S., Myers, J. S., Arnold, G. T., Platnick, S. E., Gumley, L.

E., Tsay, S. C., Moeller, C. C., Fitzgerald, M., Brown, K. S., and Osterwisch, F. G.: Airborne scanning spectrometer for remote sensing of cloud, aerosol, water vapor and surface properties, J. Atmos. Ocean. Tech., 13, 777-794, 1996.

King, M. D., Platnick, S., Wind, G., Arnold, G. T., and Dominguez, R. T.: Remote sensing of radiative and microphysical properties of clouds during TC^4: Results from MAS, MASTER, MODIS, and MISR, J. Geophys. Res, 115, D00J07, doi:10.1029/2009JD013277, 2010.

Kurucz, R. L.: Synthetic infrared spectra, in Infrared Solar Physics: Proceedings of the 154th Symposium of the International Astronomical Union, edited by D. M. Rabin, J. T. Jefferies, and C. Lindsey, pp. 523-531, Kluwer Acad., Dordrecht, Netherlands, 1992.

LeBlanc, S. E., Pilewskie, P., Schmidt, K. S., and Coddington, O. M.: A spectral method for discriminating thermodynamic phase and retrieving cloud optical thickness and effective radius using transmitted solar radiance spectra, Atmos. Meas. Tech., 8, 1361-1383, 2015.

Li, L., Heymsfield, G. M., Racette, P. E., Tian, L., and Zenker, E.: A 94 GHz cloud radar system on a NASA high-altitude ER-2 aircraft, J. Atmos. Oceanic Technol., 21, 1378-1388, 2004.

Liu, C., and Illingworth, A.: Toward more accurate retrievals of ice water content from radar measurements of clouds, J. Appl. Meteorol., 39, 1130-1146, 2000.

Loeb N. G., Kato, S., Loukachine, K., and Smith, N. M.: Angular distribution models for top-of-atmosphere radiative flux estimation from the clouds and the earth's radiant energy system instrument on the Terra satellite. Part I: Methodology, J Atmos. Oceanic Technol. 22, 338-351, 2005.

Marshak, A., and Davis, A.: 3-D Radiative Transfer in Cloudy Atmospheres, Springer, ISBN-13 978-3-540-23958-1, 2005.

Marshak, A., Platnick, S., Várnai, T., Wen, G., and Cahalan, R. F.: Impact of three-dimensional radiative effects on satellite retrievals of cloud droplet sizes, J. Geophys. Res., 111, D09207, doi:10.1029/ 996 2005JD006686, 2006.

Marshak, A., Wen, G., Coakley, J. A., Jr., Remer, L. A., Loeb, N. G., and Cahalan, R. F.: A simple model for the cloud adjacency effect and the apparent bluing of aerosols near clouds, J. Geophys. Res., 113, D14S17, doi:10.1029/2007JD009196, 2008.

Marshak, A., Wiscombe, W., Davis, A., Oreopoulos, L., and Cahalan, R.: On the removal of the effect of horizontal fluxes in two-aircraft measurements of cloud absorption, Quart. J. Roy. Meteorol. Soc., 125, 2153–2170, 1999.

Mayer, B., and Kylling, A.: Technical note: The libRadtran software package for radiative transfer calculations—Description and examples of use, Atmos. Chem. Phys., 5, 1855-1877, 2005.

Miller, S. D., Forsythe, J. M., Partain, P. T., Haynes, J. M., Bankert, R. L., Sengupta, M., Mitrescu, C., Hawkins, J. D., and Vonder Haar, T. H.: Estimating three-dimensional cloud structure via statistically blended satellite observations. J. Appl. Meteor. Climatol., 53, 437-455, 2014.

Minnis, P., Sun-Mack, S., Young, D. F., Heck, P. W., Garber, D. P., Chen, Y., Spangenberg, D. A., Arduini, R. F., Trepte, Q. Z., Smith, W. L. Jr., Ayers, J. K., Gibson, S. C., Miller, W. F., Hong, G., Chakrapani, V., Takano, Y., Liou, K. N., Xie, Y., and Yang, P.: CERES edition-2 cloud property retrievals using TRMM VIRS and Terra and Aqua MODIS data—Part I: Algorithms, IEEE Trans. Geosci. Remote Sens., 49(11), 4374–4400, 2011.

Mlawer, E., and Clough, S. A.: On the extension of rapid radiative transfer model to the shortwave region, in Proc. Sixth ARM Science Team Meeting, pp. 223–226, Atmospheric Radiation Measurement (ARM) Program, San Antonio, TX, conf–9603149, 1997.

Pilewskie, P., Pommier, J., Bergstrom, R., Gore, W., Rabbette, M., Howard, S., Schmid, B., and Hobbs, P. V.: Solar spectral radiative forcing during the South African Regional Science Initiative, J. Geophys. Res., 108, 8486, doi:10.1029/2002JD002411, 2003.

Platnick, S.: Approximations for horizontal photon transport in cloud remote sensing problems, J. Quant. Spectrosc. Radiat. Transfer, 68(1), 75-99, 2001.

Scheirer, R., and Macke, A.: Cloud inhomogeneity and broadband solar fluxes, J. Geophys. Res., 108, 4599, doi:10.1029/2002JD003321, D19, 2003.

Schmidt, K. S., Venema, V., Di Giuseppe, F., Scheirer, R., Wendisch, M., and Pilewskie, P.: Reproducing cloud microphysical and irradiance measurements using three 3D cloud generators, Quart. J. Roy. Meteorol. Soc., 133, 765-780, 2007a.

Schmidt, K. S., Pilewskie, P., Platnick, S., Wind, G., Yang, P., and Wendisch, M.: Comparing irradiance fields derived from Moderate Resolution Imaging Spectroradiometer airborne simulator cirrus cloud retrievals with solar spectral flux radiometer measurements, J. Geophys. Res., 112, D24206, doi:10.1029/2007JD008711, 2007b.

Schmidt, K. S., Pilewskie, P., Mayer, B., Wendisch, M., Kindel, B., Platnick, S., King, M. D., Wind, G., Arnold, G. T., Tian, L., Heymsfield, G., and Kalesse, H.: Apparent absorption of solar spectral irradiance in heterogeneous ice clouds, J. Geophys. Res., 115, D00J22, doi:10.1029/2009JD013124, 2010.

Schmidt, K. S., and Pilewskie, P.: Airborne Measurements of Spectral Shortwave Radiation in Cloud and Aerosol Remote Sensing and Energy Budget Studies, in Light Scattering Reviews, 6, A. Kokhanovsky (ed.), Springer, 2012.

Schmidt, K. S., Song, S., Feingold, G., Pilewskie, P., Coddington, O., 2014: Relating shortwave passive remote sensing and radiative effects if aerosol-immersed broken cloud fields, *AMS conference, Boston, July 2014*. https://ams.confex.com/ams/14CLOUD14ATRAD/webprogram/Paper250570.html

Stephens, G. L., Tsay, S.-C., Stackhouse Jr., P. W., and Flatau, P. J.: The relevance of the microphysical and radiative properties of cirrus clouds to climate and climatic feedback, J. Atmos. Sci., 47, 1742-1753, 1990.

Song, S., Schmidt, K. S., Pilewskie, P., King, M. D., and Platnick, S.: Quantifying the spectral signature of heterogeneous clouds in shortwave radiation measurements during the Studies of Emissions and Atmospheric Composition, Clouds and Climate Coupling by Regional Surveys (SEAC4RS), to be submitted to J. Geophys. Res., 2015.

Song, S.: The spectral signature of cloud spatial structure in shortwave radiation. Ph.D. thesis, University of Colorado Boulder, USA, 2016.

Titov, G. A.: Radiative horizontal transport and absorption in stratocumulus clouds, J. Atmos. Res., 55, 2549-2560. 1998.

Toon O. B., Starr, D. O., Jensen, E. J., Newman, P. A., Platnick, S., Schoeberl, M. R., Wennberg, P. O., Wofsy, S. C., Kurylo, M. J., Maring, H., Jucks, K. W., Craig, M. S., Vasques, M. F.,

Pfister, L., Rosenlof, K. H., Selkirk, H. B., Colarco, P. R., Kawa, S. R., Mace, G. G., Minnis, P., and Pickering, K. E.: Planning, implementation, and first results of the Tropical Composition, Cloud and Climate Coupling Experiment (TC^4), J. Geophys. Res., 115, D00J04, doi:10.1029/2009JD013073, 2010.

Várnai, T., and Marshak, A.: MODIS observations of enhanced clear sky reflectance near clouds, Geophys. Res. Lett., 36, L06807, doi:10.1029/2008GL037089, 2009.

Walther, A., and Heidinger, A.: Implementation of the Daytime Cloud Optical and Microphysical Properties Algorithm (DCOMP) in PATMOS-x. J. Appl. Meteor. Climatol., 51, 1371-1390, 2012.

Welch, R. M., Cox, S. K. and Davis, J. M.: Solar Radiation and Clouds. Meteor. Monogr., No. 39, Amer. Meteor. Soc., 93 pp., 1980.

Wen, G., Marshak, A., Cahalan, R. F., Remer, L. A., and Kleidman, R. G.: 3-D aerosol-cloud radiative interaction observed in collocated MODIS and ASTER images of cumulus cloud fields, J. Geophys. Res.,112, D13204, doi:10.1029/2006JD008267, 2007.

Wielicki, B. A., Barkstrom, B. R., Harrison, E. F., Lee, R. B., Smith, G. L., and Cooper, J. E.: Clouds and the Earth's Radiant Energy System (CERES): An Earth Observing System Experiment, Bull. Amer. Meteor. Soc., 77, 853-868, 1996.

Wiscombe, W. J., Welch, R. M., and Hall, W. D.: The effects of very large drops on cloud absorption, part I: Parcel models, J. Atmos. Sci., 41, 1336-1355, 1984.

Atmos. Chem. Phys. Discuss., doi:10.5194/acp-2015-911, 2016
Manuscript under review for journal Atmos. Chem. Phys.
Published: 14 March 2016

Atmospheric Chemistry and Physics Discussions

Table 1. Cloud optical thickness τ, effective radius r_e, and values of H_0 and S_0 for the eight pixels highlighted in Fig. 1 (sorted by H_0). For pixels 5, 6, 7, 8, Fig. 3a shows the spectral shape of H_λ.

Pixel	τ	r_e (µm)	H_0 (%)	S_0 (%/100 nm)
6	10.3	27.5	28.92	2.36
1	13.0	30.1	21.17	1.56
3	21.2	30.0	13.04	1.08
2	18.1	30.6	9.92	1.63
5	12.2	27.5	4.95	0.48
7	8.0	27.8	–5.18	-0.78
4	11.8	28.2	–18.7	–1.54
8	7.7	24.2	–24.13	–2.46

Atmos. Chem. Phys. Discuss., doi:10.5194/acp-2015-911, 2016
Manuscript under review for journal Atmos. Chem. Phys.
Published: 14 March 2016

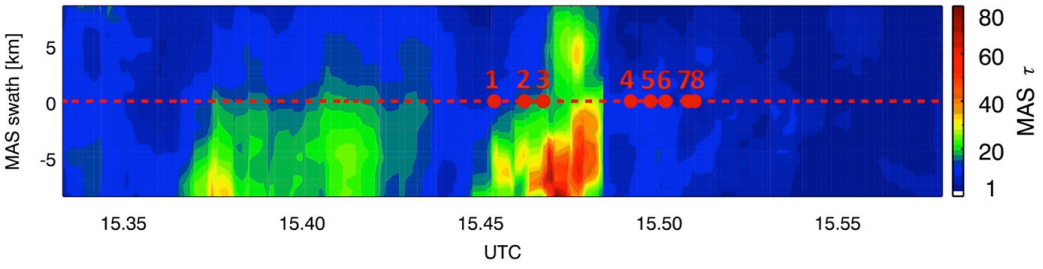

Fig. 1. Cloud optical thickness from MAS along an ER-2 leg from 17 July 2007 (length: 192 km, swath: 17.5 km), regridded to a horizontal resolution of 500 m. The red dashed line indicates the ER-2 flight track in the center of the MAS swath. Results of net horizontal photon transport for the eight highlighted pixels are shown in Table 1 and Fig. 3a.

Atmos. Chem. Phys. Discuss., doi:10.5194/acp-2015-911, 2016
Manuscript under review for journal Atmos. Chem. Phys.
Published: 14 March 2016

Atmospheric Chemistry and Physics Discussions

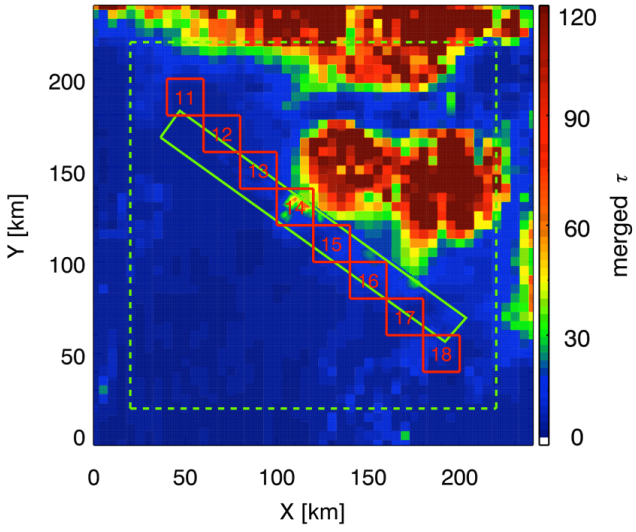

Fig. 2. Optical thickness of the large-scale cloud field. The green rectangle marks the embedded MAS swath (Fig. 1); the red squares mark 20 km "super-pixels" within the scene. Radiative transfer model output outside the dashed green square is discarded (see Section 7).

Atmos. Chem. Phys. Discuss., doi:10.5194/acp-2015-911, 2016
Manuscript under review for journal Atmos. Chem. Phys.
Published: 14 March 2016

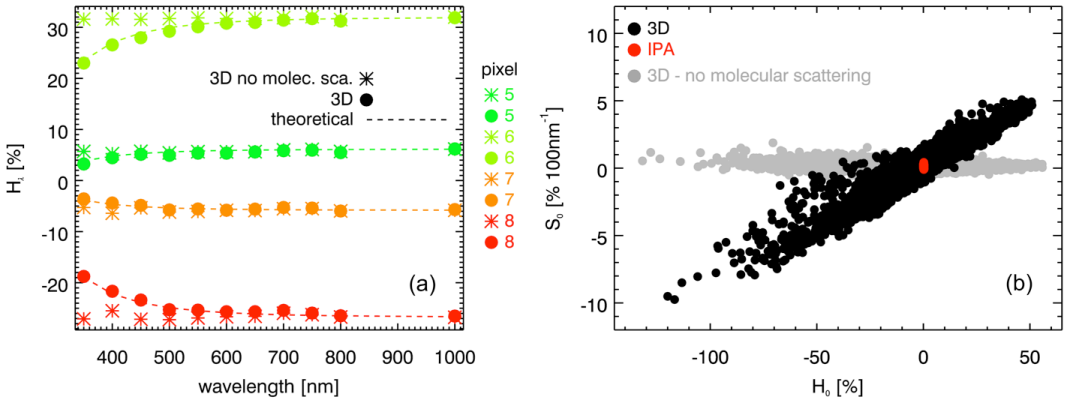

Fig. 3. (a) The H_λ spectra of pixels {5,6,7,8} from Fig. 1 and Table 1 with (•) and without (∗) molecular scattering in the 3D calculations, as well as a fit based on Eq. (12) from Section 6 (dashed lines). (b) Spectral slope (S_0) vs. net horizontal photon transport (H_0) from (a) (both at 500 nm) for all the pixels from Fig. 1. Only 3D calculations with molecular scattering (black dots) show the systematic correlation between H_0 and S_0. Disabling molecular scattering (grey dots) incorrectly predicts a spectrally neutral (flat) H_λ ($S_0 \approx 0$ for all pixels). By definition, 1D calculations (IPA, red dots) do not reproduce net horizontal photon transport at all ($H_0 = 0$ for all pixels).

Atmos. Chem. Phys. Discuss., doi:10.5194/acp-2015-911, 2016
Manuscript under review for journal Atmos. Chem. Phys.
Published: 14 March 2016

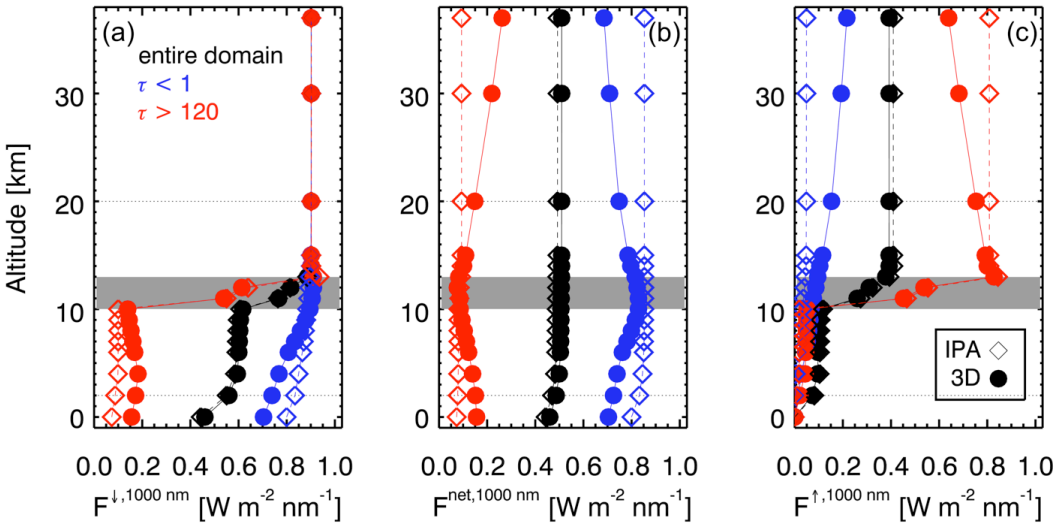

Fig. 4. Profiles of (a) downwelling, (b) net, and (c) upwelling irradiance at 1000 nm for the cloud field from Fig. 1. The location of the cloud layer is marked in grey. Both IPA (dashed line, hollow symbols) and 3D calculations (solid line, full symbols) are shown, averaged over the full domain (black), over all columns with $\tau < 1$ (blue) and over columns with τ. 120 (red).

Atmos. Chem. Phys. Discuss., doi:10.5194/acp-2015-911, 2016
Manuscript under review for journal Atmos. Chem. Phys.
Published: 14 March 2016

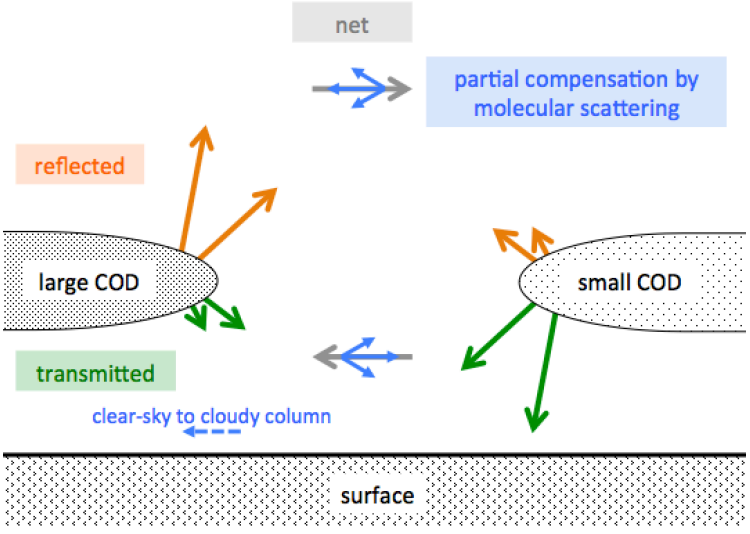

Fig. 5. Conceptual visualization of the mechanism of horizontal photon transport.

Atmos. Chem. Phys. Discuss., doi:10.5194/acp-2015-911, 2016
Manuscript under review for journal Atmos. Chem. Phys.
Published: 14 March 2016

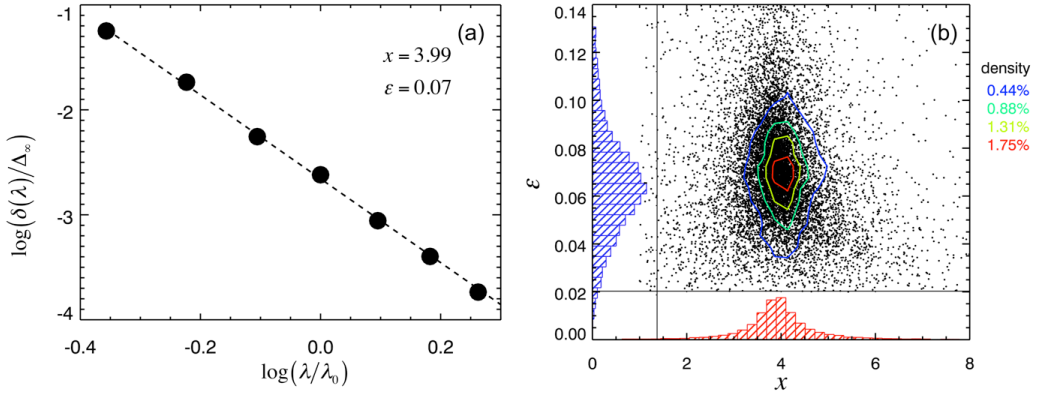

1

2 **Fig. 6.** (a) An example of the linear regression between $\log\frac{\delta(\lambda)}{H_\infty}$ versus $\log\frac{\lambda}{\lambda_0}$, from which the

3 values of x and ε can be derived. (b) The scatter plot of x versus ε for all pixels, joint PDFs $p(x,\varepsilon)$

4 (contours) as well as the marginal PDFs $p(x)$ and $p(\varepsilon)$ (histograms). The peak of $p(x,\varepsilon)$, and thus

5 the most likely values $\{x,\varepsilon\}$ values for the cloud field is located at $\{3.85, 0.065\}$, and the domain-

6 averaged values are $\{3.91, 0.070\}$.

Atmos. Chem. Phys. Discuss., doi:10.5194/acp-2015-911, 2016
Manuscript under review for journal Atmos. Chem. Phys.
Published: 14 March 2016

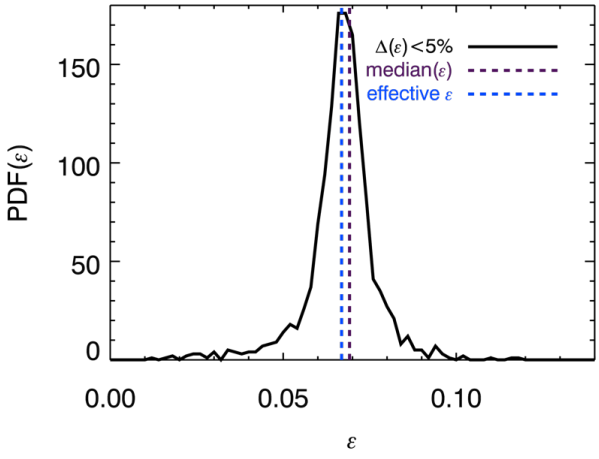

Fig. 7. PDF of ε for all pixels with $\Delta(\varepsilon) < 5\%$, median (purple dashed line), and domain-wide *effective* ε derived from regression of S_0 vs. H_∞ (blue dashed line).

Atmos. Chem. Phys. Discuss., doi:10.5194/acp-2015-911, 2016
Manuscript under review for journal Atmos. Chem. Phys.
Published: 14 March 2016

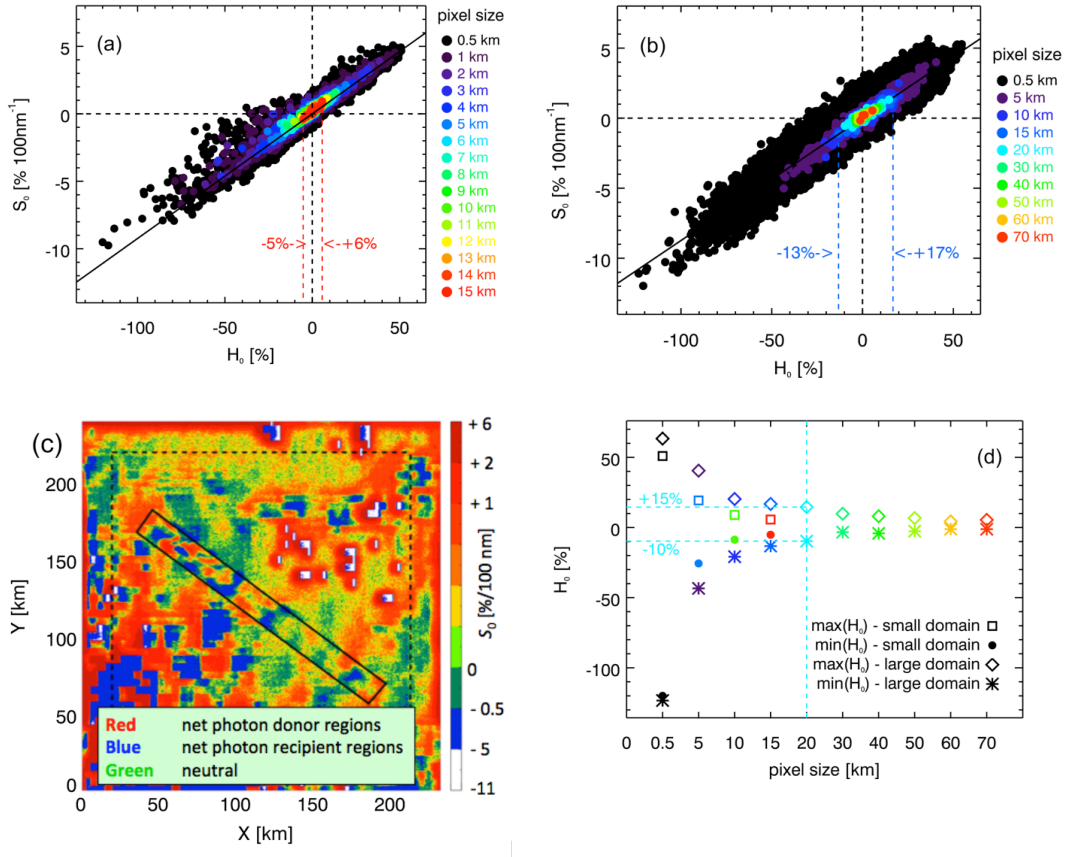

1 **Fig. 8**. Scatter plot of S_0 versus H_0 as obtained from linear regression of Eq. (12) for (a) the small
2 domain from Fig. 1 and (b) the large-scale domain from Fig. 2, spatially aggregated to different
3 scales, including the 20 km "super pixels" as highlighted in Fig. 2 (red squares). The dashed lines
4 indicate the range for 15 km pixels. (c) Spatial distribution of S_0 from (b). Red (blue) indicates
5 net photon "donor" ("recipient") pixels, and green "neutral zones" ($H_\lambda \approx S_0 \approx 0$). (d) Dependence
6 of max(H) and min(H) on spatial aggregation scale (km). The color is the same as in (b).

Atmos. Chem. Phys. Discuss., doi:10.5194/acp-2015-911, 2016
Manuscript under review for journal Atmos. Chem. Phys.
Published: 14 March 2016

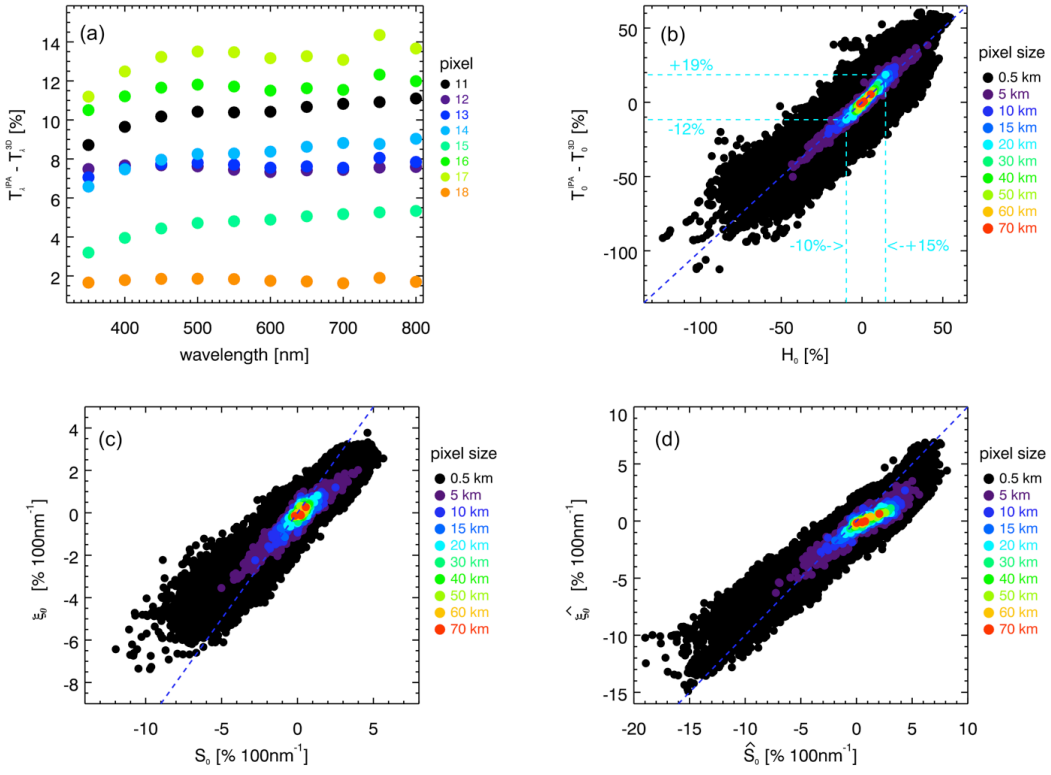

1 **Fig. 9.** (a) Transmittance biases (IPA-3D transmittance) for the eight super-pixels from Fig. 2. (b)
2 Correlation between net horizontal photon transport from Fig. 8b and transmittance bias for
3 multiple spatial aggregation scales. The dashed lines indicate the range of variability for 20 km
4 super-pixel size. (c) Correlation of the *slopes* of the quantities from (b). (d) Same as (c), but for a
5 bracket from the surface to cloud top, rather than the cloud layer only.

Atmos. Chem. Phys. Discuss., doi:10.5194/acp-2015-911, 2016
Manuscript under review for journal Atmos. Chem. Phys.
Published: 14 March 2016

Atmospheric Chemistry and Physics Discussions

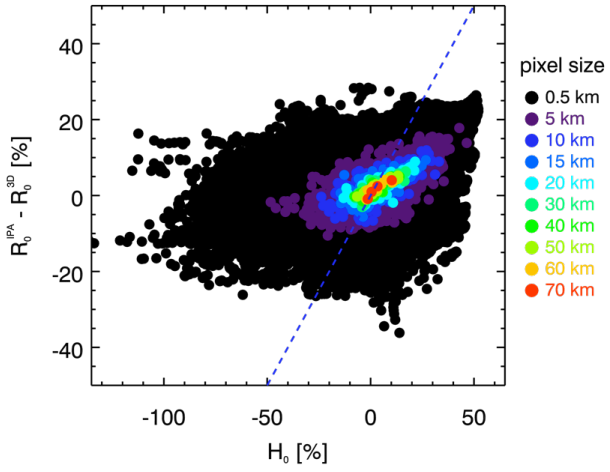

Fig. 10. H_0 is only weakly correlated with reflectance biases ΔR_0 (IPA-3D reflectance) at scales below 15 km, which means that, statistically, biases introduced by horizontal photon transport propagate primarily into transmittance, not albedo. This changes for larger scales.